Applied Mathematics & Information Sciences Letters
An International Journal

http://dx.doi.org/10.18576/amisl/140102

Enhancing Fire Extinguishing Efficiency Using Nanofluid Flow through Porous Sprayers

Michael H. Mkwizu[1,*] *and Alex X. Matofali*[1]

[1] Department of Mathematics and Statistics, College of Natural and Applied Sciences, Sokoine University of Agriculture, Morogoro-Tanzania

Received: 5 Sep. 2025, Revised: 1 Oct. 2025, Accepted: 28 Nov. 2025
Published online: 1 Jan. 2026

Abstract: This study investigates the enhancement of fire extinguishing efficiency through nanofluid flow within a porous sprayer. Water-based nanofluids containing magnesium hydroxide ($Mg(OH)_2$) and zinc oxide (ZnO) nanoparticles are considered. The governing equations describing one-dimensional flow through the porous medium are solved numerically using MATLAB, employing a Runge–Kutta–Fehlberg scheme. The analysis focuses on the effects of key flow parameters on velocity, temperature distribution, skin friction, and entropy generation. Results indicate that $Mg(OH)_2$-based nanofluids exhibit higher velocities and temperatures compared to ZnO-based nanofluids under similar conditions. In addition, entropy generation decreases with increasing nanoparticle volume fraction for both nanofluids, indicating improved thermodynamic efficiency. Skin friction shows only minor variation between the two nanofluids, suggesting comparable resistance characteristics within the porous structure. These upstream hydrodynamic results are interpreted in the context of fire suppression, where higher exit velocities and reduced entropy generation are associated with improved spray formation and enhanced heat removal capability. The findings highlight the potential of nanofluids to improve cooling efficiency and support more effective fire extinguishing through optimized porous sprayer design.

Keywords: Nanofluids, fire extinguish, porous sprayers

1 Introduction

Fire-extinguishing systems that rely on water sprays including low-pressure sprinklers and high-efficiency water-mist systems remain the most widely used active fire-protection method. This prevalence is due to water's high specific heat capacity and large latent heat of vaporization, which enable it to lower flame temperatures and suppress the release of combustible vapors near the flame front [1]. The performance of a water spray is strongly influenced by factors such as droplet-size distribution, spray flux, nozzle geometry, droplet momentum, and residence time. While smaller droplets provide a higher surface-area-to-mass ratio, improving heat absorption and evaporation those that are too small may be swept away by buoyant hot gases before contributing effectively to suppression. Consequently, both numerical and experimental investigations consistently demonstrate that optimizing spray characteristics by reducing droplet size and refining nozzle design can shorten extinguishment time and enhance temperature-decay rates [2]. The selection of fire-extinguishing agents is a fundamental component of fire-protection engineering, and these agents continue to evolve as new technologies emerge to better protect people, property, and critical infrastructure. In recent years, nanotechnology has significantly advanced extinguishing media, offering enhanced efficiency and responsiveness. Due to their exceptionally high surface-area-to-volume ratios, nanoparticles can rapidly adsorb combustion products and facilitate accelerated chemical reactions. Research further shows that certain nanoparticles generate reactive oxygen species capable of degrading organic and toxic fire emissions into simpler, less harmful compounds. Consequently, nanomaterial-based extinguishing agents offer promising potential to limit smoke spread and reduce hazardous by-products, thereby decreasing risks to human health and safety in fire environments [3,4]. Nanofluids are advanced colloidal mixtures consisting of nanoparticles commonly metal oxides or carbon-based materials dispersed in traditional base fluids such as water, ethylene

* Corresponding author e-mail: mkwizu@sua.ac.tz

glycol, or oil. The incorporation of nanoparticles enhances the fluid's thermal conductivity, convective heat-transfer performance, and viscosity due to their high surface-area-to-volume ratio and superior thermal properties. These improvements in thermophysical behavior make nanofluids highly suitable for high-performance cooling systems, heat exchangers, and other industrial thermal applications. Consequently, nanofluids represent a modern and efficient solution for advanced thermal management and energy systems [5,6]. Research from spray-cooling and droplet-combustion studies offers valuable insights applicable to firefighting technologies. Laboratory investigations on nanofluid sprays and single-droplet behavior have reported mixed but often beneficial outcomes. Nanofluids have been shown to increase critical heat flux in spray-cooling systems, shift the Leidenfrost temperature, and modify droplet spreading and evaporation on heated surfaces. In combustion settings, introducing nanoparticles into fuel droplets can enhance radiative absorption within the liquid, accelerating vaporization and altering burning rates. These findings demonstrate that nanoparticles significantly influence energy exchange at both liquid gas and liquid–solid interfaces [6,7]. These findings imply that nanofluid droplets used in fire-suppression sprays may improve heat removal from flames and hot surfaces per unit mass of liquid delivered. However, the same radiative-absorption mechanisms that improve cooling could, under certain conditions, also intensify fuel vaporization and locally increase burning rates. Consequently, the net extinguishing performance depends strongly on the fire type, nanoparticle characteristics, and operating conditions [7]. The spray-cooling and droplet-combustion literature provides valuable insights applicable to firefighting technologies. Laboratory investigations involving nanofluid sprays and single-droplet experiments have shown mixed but often favorable outcomes. For instance, nanofluids have been found to increase the critical heat flux in spray-cooling systems, shift the Leidenfrost temperature, and alter droplet spreading and evaporation behavior on heated surfaces [8,9] In combustion environments, introducing nanoparticles into fuel droplets can enhance radiative absorption within the liquid, accelerating vaporization and modifying burning rates. This demonstrates the strong influence nanoparticles exert on energy exchange at liquid–gas and liquid–solid interfaces. These observations suggest that nanofluid droplets deployed in fire-suppression sprays may improve heat removal from flames and hot surfaces per unit mass of liquid delivered. However, the same radiative-absorption mechanisms that enhance cooling may, under certain conditions, promote fuel vaporization and locally intensify burning. Consequently, the overall extinguishing performance depends greatly on the fire type, nanoparticle properties, and operating conditions [7,10]. Recent experimental work focused specifically on nanofluid sprays (including alumina- and carbon-based colloids) demonstrates improvements in spray-cooling metrics and suppression thresholds: some studies report higher critical suppression temperatures and delayed thermal runaway when using nanofluid sprays compared with water alone. Numerical analyses of water-mist suppression emphasize the importance of droplet size distributions and local spray characteristics; integrating nanofluid-specific thermophysical properties into these models has begun to show potential performance gains but remains an area of active research [10]. Porous sprayers and specialized nozzles are commonly employed to generate fine water mist with a narrow droplet-size distribution. By enhancing sheet breakup and droplet atomization, the porous-medium design produces a large number of small droplets for a given mass flow-a characteristic highly desirable for effective fire suppression [11]. Introducing nanofluids into porous sprayers, however, raises several practical considerations, including the risk of particle filtration or clogging within the pores, the stability of the colloidal suspension under shear and high pressure, and the potential for nanoparticle agglomeration during atomization. Existing studies report both promising results and technical constraints: appropriately stabilized nanofluids can be atomized without immediate agglomeration, yet ensuring long-term system reliability and preventing nozzle fouling require careful formulation and material selection [7,12]. The application of nanoparticles in fire suppression raises important environmental and health questions that must be addressed alongside performance goals. While studies and review articles on nanotechnology in extinguishing agents discuss potential benefits such as reduced water demand and faster suppression, they also emphasize the need to assess toxicity, downstream water contamination, inhalation exposure to aerosolized particles, and regulatory acceptability. Consequently, designing nanofluids that balance suppression performance with benign environmental profiles for instance, by using low-toxicity metal oxides or biodegradable surface modifiers represents an essential parallel research track [13].

[14] conducted an experimental study on enhanced heat transfer through nanoparticle deposition using TiO_{x_2}–water nanofluid sprays. Their results showed that nanofluid sprays improved heat transfer by initially coating the heated surface and subsequently maintaining an optimal coating through continuous nanoparticle deposition. To the best of the authors' knowledge, this study is the first in nanofluid spray cooling to demonstrate heat-transfer enhancement resulting from increased nucleation sites due to self-sustained nanoparticle deposits. This finding highlights the potential for implementing nanofluid sprays in industrial applications without the need for a durable coating.

[15] conducted a study titled Nanofluids for Sustainable Heat Transfer Enhancement: Beyond Thermal Conductivity. The results indicate that thermal conductivity alone cannot fully explain the observed

performance improvements. Instead, mechanisms such as Brownian motion, induced convection, dynamic wetting, and nanoparticle-driven surface modification play significant roles. These factors influence droplet impact dynamics, spreading behavior, boiling transitions, and transient heat transfer during impact and evaporation.

Unlike previous studies that examine either spray cooling or nanofluid channel flow independently, this work integrates nanofluid transport through porous sprayers with entropy analysis for fire-extinguishing applications. To address this gap, the study investigates whether nanofluid porous-sprayer systems can provide more water-efficient fire-extinguishing solutions, as discussed by [10].

2 Mathematical Model

2.1 Physical Description

This study considers the unsteady flow of a nanofluid through a porous sprayer channel representing the internal flow within a fire-suppression nozzle. The nanofluid consists of water as the base fluid with suspended nanoparticles of magnesium hydroxide (Mg (OH) 2) and zinc oxide (ZnO). The present model describes nanofluid transport within a porous sprayer/nozzle as a one-dimensional internal flow. While it does not resolve external spray dynamics such as atomization, droplet-size distribution, or spray footprint, it provides key inlet conditions that govern these processes. Specifically, the model predicts exit velocity, temperature, nanoparticle concentration, and entropy generation, which directly influence atomization quality and thermal performance. Higher exit momentum and optimized thermophysical properties can promote finer droplet formation, increased surface area, and improved cooling/heat absorption during fire suppression. The fluid flows through a channel featuring Navier slip, permeability, and convective cooling at the upper wall, as illustrated in Figure 1.
The governing one-dimensional momentum and energy equations for the nanofluid can be expressed as follows:

$$\frac{\partial u}{\partial \bar{t}} + V\frac{\partial u}{\partial y} = -\frac{1}{\rho_{nf}}\frac{\partial P}{\partial x} + \frac{\mu_{nf}}{\rho_{nf}}\frac{\partial^2 u}{\partial y^2} \tag{1}$$

$$\frac{\partial u}{\partial \bar{t}} + V\frac{\partial u}{\partial y} = -\frac{1}{\rho_{nf}}\frac{\partial P}{\partial x} + \frac{\mu_{nf}}{\rho_{nf}}\frac{\partial^2 u}{\partial y^2} \tag{2}$$

where u is the nanofluid velocity in the x-direction, T is the nanofluid temperature, p is the nanofluid pressure, t is time, H is the channel width, T_w is the temperature of the lower stationary wall, μ_{nf} is the dynamic viscosity of the nanofluid, k_{nf} is the nanofluid thermal conductivity, ρ_{nf} is the nanofluid density, and α_{nf} is the thermal diffusivity of the nanofluid.

The nanoparticles volume fraction is represented by ϕ ($\phi = 0$) corresponds to a base fluid). The symbols ρ_f and

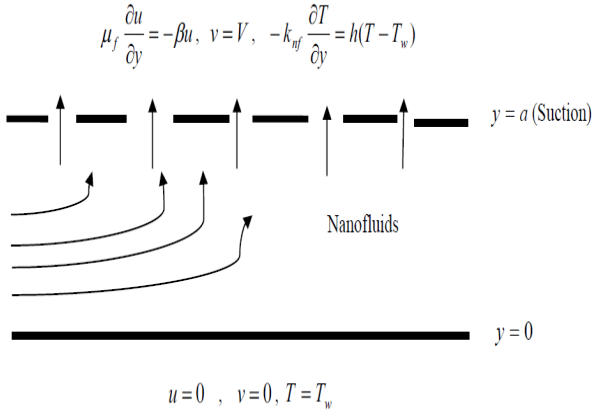

Fig. 1: Schematic diagram of the problem under consideration

ρ_s denote the densities of the base fluid and the nanoparticle, respectively, while k_f and k_s represent their thermal conductivities. Similarly, $(\rho c_p)_f$ and $(\rho c_p)_s$ denote the heat capacitances of the base fluid and the nanoparticle, respectively. In addition, β is defined for spherical nanoparticles and does not account for non-spherical particle shapes. The effective viscosity of the nanofluid μ_{nf} corresponds to the viscosity of a base fluid containing a dilute suspension of fine spherical particles. The initial and boundary conditions are defined as follows:

$$u(y,0) = 0, \quad T(y,0) = T_w, \tag{3}$$

$$u(0,\bar{t}) = 0, \quad T(0,\bar{t}) = T_w \tag{4}$$

$$\mu_f \frac{\partial u}{\partial \bar{t}}(a,\bar{t}) = -\beta u(a,\bar{t}), \tag{5}$$

$$-k_{nf}\frac{\partial T}{\partial y}(a,\bar{t}) = h\left(T(a,\bar{t}) - T_w\right) \tag{6}$$

Table 1 presents the thermophysical properties of water, magnesium hydroxide (Mg(OH)x_2), and zinc oxide (ZnO). The selected range of nanoparticle volume fraction is determined by a balance between thermodynamic enhancement and hydrodynamic stability. At low to moderate concentrations, the addition of nanoparticles increases the effective thermal conductivity, thereby reducing entropy generation and improving heat transfer efficiency. However, beyond a critical volume fraction, particle–particle interactions become significant, leading to agglomeration and a sharp increase in effective viscosity. In addition, the nanoparticles considered in this study contribute to fire suppression through distinct physicochemical mechanisms. Magnesium hydroxide (Mg(OH)x_2) undergoes an endothermic decomposition reaction, releasing water vapor while absorbing a substantial amount of thermal energy.

Table 1: Thermophysical properties of the selected nanoparticles and the base fluid (water)

Physical properties	Fluid phase (water)	$Mg(OH)_2$	ZnO
c_p (J/kg K)	4179	1323	495.2
ρ (kg/m^3)	997.1	2410	5600
k (W/m K)	0.613	0.06562	13

The dimensionless variables and parameters are defined as follows:

$$\left.\begin{aligned} &\theta = \frac{T-T_w}{T_w}, \quad W = \frac{u}{U}, \quad t = \frac{\bar{t}V}{a}, \upsilon_f = \frac{\mu_f}{\rho_f}, \\ &\bar{P} = \frac{Pa}{\mu_f U}, \quad A = -\frac{\partial \bar{P}}{\partial X}, \quad X = \frac{x}{a}, \quad \eta = \frac{y}{a}, \\ &m = \frac{(k_s+2k_f)+\varphi(k_f-k_s)}{(k_s+2k_f)-2\varphi(k_f-k_s)}, \quad Re = \frac{Va}{\upsilon_f}, \\ &\alpha_f = \frac{k_f}{(\rho c_p)_f}, \quad f = \frac{\mu_f}{\beta a} \end{aligned}\right\} \tag{7}$$

The dimensionless governing equations, together with the appropriate initial and boundary conditions, can be expressed as:

$$\frac{\partial W}{\partial t} = \frac{A}{Re\left(1-\varphi+\frac{\varphi\rho_s}{\rho_f}\right)} + \frac{1}{Re\left(1-\varphi+\frac{\varphi\rho_s}{\rho_f}\right)(1-\varphi)^{2.5}}\frac{\partial^2 W}{\partial \eta^2} - \frac{\partial W}{\partial \eta} \tag{8}$$

$$\frac{\partial \theta}{\partial t} = \frac{1}{mPrRe\,(1-\varphi+\varphi\tau)}\frac{\partial^2 \theta}{\partial \eta^2} + \frac{Ec}{Re\,(1-\varphi)^{2.5}(1-\varphi+\varphi\tau)}\left(\frac{\partial W}{\partial \eta}\right)^2 - \frac{\partial \theta}{\partial \eta} \tag{9}$$

with the initial and boundary conditions

$$W(\eta,0) = 0, \quad \theta(\eta,0) = 0 \tag{10}$$

$$W(0,t) = 0, \quad \theta(0,t) = 0 \tag{11}$$

$$\frac{\partial W}{\partial \eta}(1,t) = -\frac{\beta a}{\mu_f} W(1,t), \quad \frac{\partial \theta}{\partial \eta}(1,t) = -mBi\theta(1,t) \tag{12}$$

where Pr is the Prandtl number, Ec is the Eckert number, Re is the Reynolds number, A is the pressure gradient parameter, λ is the coefficient of sliding friction, and β is the slip parameter. Other physical quantities of practical interest in this study are the skin friction coefficient C_f and the local Nusselt number Nu, which are defined as

$$C_f = \frac{a\tau_w}{\mu_f U}, \quad Nu = \frac{aq_w}{k_f T_w} \tag{13}$$

where τ_w is the wall shear stress and q_w is the heat flux at the channel walls given by

$$\tau_w = -\mu_{nf}\left.\frac{\partial u}{\partial y}\right|_{y=a}, \quad q_w = -k_{nf}\left.\frac{\partial T}{\partial y}\right|_{y=a} \tag{14}$$

Substituting equations (14) into (13) and using dimensionless variables, we obtain

$$\left.\begin{aligned} C_f &= -\frac{1}{(1-\varphi)^{2.5}}\frac{\partial W}{\partial \eta} \\ Nu &= -\frac{1}{m}\frac{\partial \theta}{\partial \eta} \end{aligned}\right\} \quad \text{at} \quad \eta = 1 \tag{15}$$

3 Entropy Analysis

The second law of thermodynamics provides a fundamental framework for analyzing irreversibility effects arising from flow and heat transfer. Thermodynamic irreversibility is closely associated with entropy generation. Convection processes involving nanofluid flow through a channel are inherently irreversible due to the exchange of energy and momentum within the nanofluid and at the solid boundaries. The local volumetric rate of entropy generation is expressed as follows:

$$S''' = \frac{k_{nf}}{T_w^2}\left(\frac{\partial T}{\partial y}\right)^2 + \frac{\mu_{nf}}{T_w}\left(\frac{\partial u}{\partial y}\right)^2 \tag{16}$$

The first term in Equation (16) represents entropy generation due to heat transfer, while the second term corresponds to entropy generation caused by nanofluid friction. By employing the dimensionless variables defined in Equation (7), the entropy generation number can be expressed in dimensionless form as follows:

$$Ns = \frac{a^2 S'''}{k_f} = \frac{1}{m}\left(\frac{\partial \theta}{\partial \eta}\right)^2 + \frac{Br}{(1-\varphi)^2}\left(\frac{\partial W}{\partial \eta}\right)^2 \tag{17}$$

Where $Br = EcPr$ is the Brinkman number. The Bejan number Be is define as

$$Be = \frac{N_1}{N_s} = \frac{1}{1+\Phi} \tag{18}$$

where $N_s = N_1 + N_2$ and

$N_1 = \frac{1}{m}\left(\frac{\partial \theta}{\partial \eta}\right)^2$ – The entropy generation due to heat transfer

$N_2 = \frac{Br}{(1-\varphi)^2}\left(\frac{\partial W}{\partial \eta}\right)^2$

The entropy generation due to fluid friction

The irreversibility distribution ratio is defined as $\Phi = N2/N1$. Heat transfer irreversibility dominates when $0 \leq \Phi < 1$ while fluid friction irreversibility dominates for $\Phi > 1$. Both irreversibilities contribute equally to entropy generation when $\Phi = 1$. Equation (18) indicates that the Bejan number ranges from 0 to 1. A Bejan number of zero corresponds to a flow system where irreversibility is dominated by fluid friction, whereas a Bejan number of one corresponds to the case where heat transfer irreversibility dominates. The contributions of both heat transfer and fluid friction to the overall irreversibility are equal when $Be = 0.5$.

4 Numerical Procedure

The nonlinear initial-boundary value problem (IBVP) in equations (8)-(18) is solved numerically via a semi-discretization finite difference method. This involves discretizing the spatial domain on a uniform Cartesian grid. The first and second spatial derivatives appearing in equations (8) and (9) are approximated using second-order central finite differences

$$\frac{\partial W_i}{\partial t} = \frac{A}{Re\left(1-\varphi+\frac{\varphi\rho_s}{\rho_f}\right)} + \frac{(W_{i+1}-2W_i+W_{i-1})}{Re\left(1-\varphi+\frac{\varphi\rho_s}{\rho_f}\right)(1-\varphi)^{2.5}(\Delta\eta)^2} - \frac{W_{i+1}-W_{i-1}}{2\Delta\eta} \tag{19}$$

$$\frac{\partial \theta_i}{\partial t} = \frac{(\theta_{i+1}-2\theta_i+\theta_{i-1})}{mPrRe(1-\varphi+\varphi\tau)(\Delta\eta)^2} + \frac{Ec}{Re(1-\varphi)^{2.5}(1-\varphi+\varphi\tau)}\left(\frac{W_{i+1}-W_{i-1}}{\Delta\eta}\right)^2 - \frac{\theta_{i+1}-\theta_{i-1}}{2\Delta\eta} \tag{20}$$

with initial conditions and boundary conditions

$$W_i(0) = \theta_i(0) = 0, \quad 1 \le i \le N+1 \tag{21}$$

$$W_1 = \frac{-fW_2}{\Delta\eta - f}, \quad \theta_1 = 0, W_{N+1} = 0, \tag{22}$$

$$\theta_{N+1} = \theta_N(1 - mBi\Delta\eta) \tag{23}$$

Given that equations (19)-(23) constitute a system of first-order ordinary differential equations with known initial conditions, they are well-suited for iterative solution via the Runge-Kutta-Fehlberg integration technique, implemented computationally in MATLAB. Through this numerical process, the skin-friction coefficient defined in (15) is also calculated, and the corresponding results are presented.

5 Results and Discussions

Figure 2-13 presents the numerical results for the representative velocity field, temperature field, entropy generation rate, and skin friction. These computations are based on specific, arbitrarily chosen values for the thermophysical parameters governing the flow system. The Prandtl number for the base fluid (pure water) is fixed at 6.2, and the effect of solid volume fraction is investigated across the range $0 \le \phi \le 0.3$. A detailed discussion and graphical representation of these results are provided in this section.

5.1 Effects of parameter variation on velocity profiles

The effects on the nanofluid velocity profiles are clearly revealed in Figure 2-6. As shown, the velocity increases with both time and space. Furthermore, it is noted that the magnesium hydroxide-water nanofluid yields a higher velocity than the zinc oxide-water nanofluid. This enhancement may be attributed to differences in their thermophysical properties. Figure 3 reveals that velocity

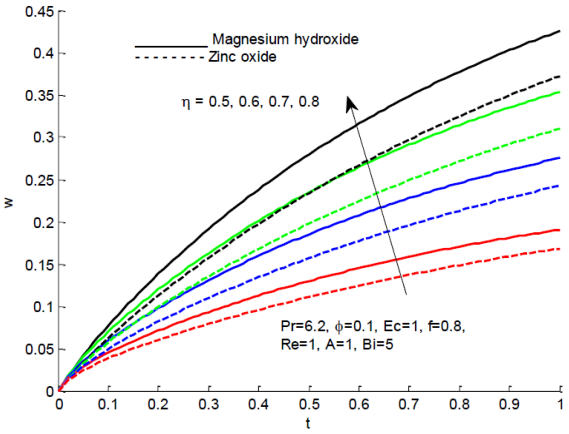

Fig. 2: Nanofluids velocity profiles with increasing time

increases with time but decreases with space for both magnesium hydroxide-water and zinc oxide-water nanofluids. Furthermore, the magnesium hydroxide-water nanofluid attains a higher velocity than the zinc oxide-water nanofluid, which may be attributed to its distinct thermophysical properties.
Figures 4-6 illustrate how parameter variations affect velocity profiles in a magnesium hydroxide-water nanofluid. The results demonstrate that velocity decreases with an increasing nanoparticle volume fraction (ϕ) increases, due to the associated rise in fluid density. Conversely, velocity increases with a higher-pressure gradient (A). Furthermore, an increase in the slip parameter (f) reduces the velocity, while a value of zero results in no change. This confirms that the slip parameter exerts a resistive effect on the nanofluid flow.

5.2 Effects of parameter variation on temperature profiles

The transient effects on the nanofluid temperature profiles are clearly revealed in Figures 7-11. Figure 7 shows that temperature increases with both time and space.

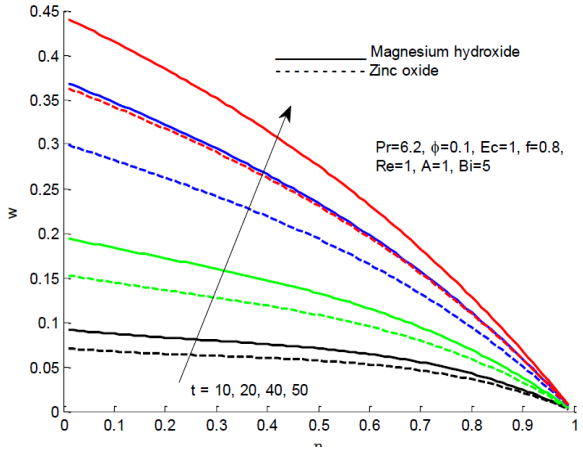

Fig. 3: Nanofluids velocity profiles across the channel with increasing time

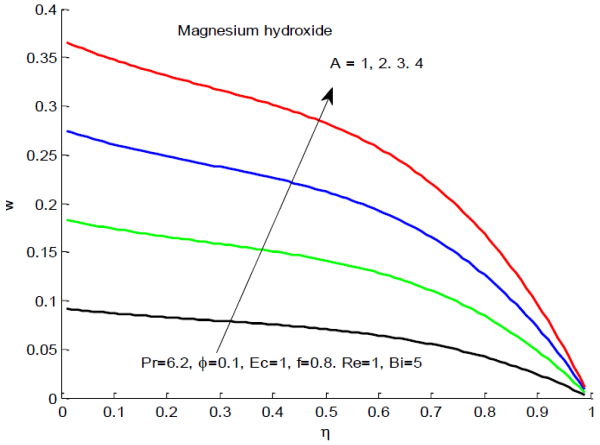

Fig. 5: Nanofluids velocity profiles with increasing A

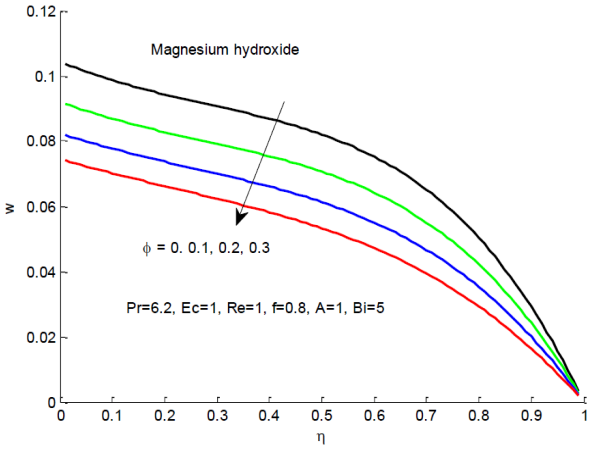

Fig. 4: Nanofluids velocity profiles with increasing ϕ

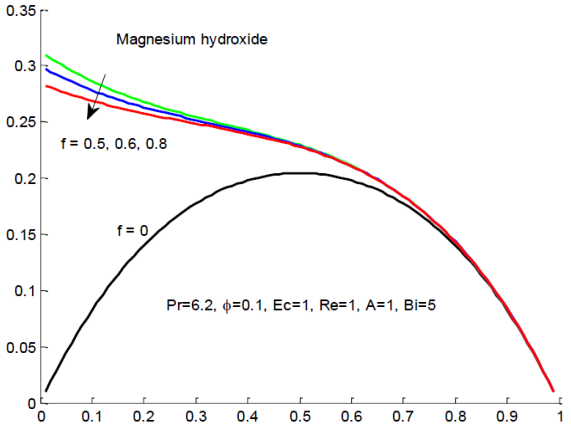

Fig. 6: Nanofluids velocity profiles with increasing f

Furthermore, the magnesium hydroxide-water nanofluid exhibits a higher temperature than the zinc oxide-water nanofluid, likely due to its distinct thermophysical properties.

Figure 8 indicates a temperature increase with both space and time. Furthermore, a marked difference in temperature elevation is observed between the two nanofluids, with the magnesium hydroxide-water mixture showing a more pronounced increase than the zinc oxide-water mixture a phenomenon likely due to its specific thermophysical properties. Figures 9-11 illustrate parameter effects on temperature profiles for a magnesium hydroxide-water nanofluid. In Figure 9, a higher Biot number (Bi) results in a nearly constant temperature profile, with a slight increase only near the upper plate. Figure 10 shows that increasing the nanoparticle volume fraction (ϕ) raises the temperature at the centerline but causes a slight decrease near the upper plate. Finally, Figure 11 indicates that a rise in the Eckert number (Ec) increases the temperature due to convective cooling at the upper wall.

5.3 Effects of Parameter Variation on the Entropy Generation Rate

Figure 10 illustrates the influence of nanoparticle volume fraction on entropy generation within the upstream flow system. As the volume fraction increases, the $Mg(OH)_2$-based nanofluid exhibits higher entropy generation than the ZnO-based nanofluid. This behavior is attributed to differences in effective thermophysical properties, particularly viscosity and thermal conductivity, which modify the balance between viscous dissipation and heat transfer irreversibility. The comparatively lower entropy generation observed for ZnO indicates reduced thermodynamic losses and more

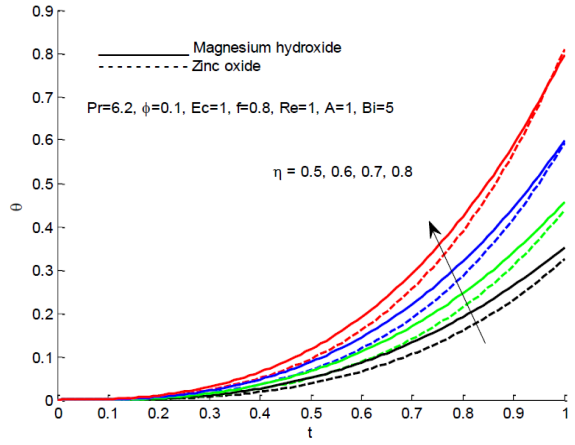

Fig. 7: Nanofluids temperature profiles with increasing time

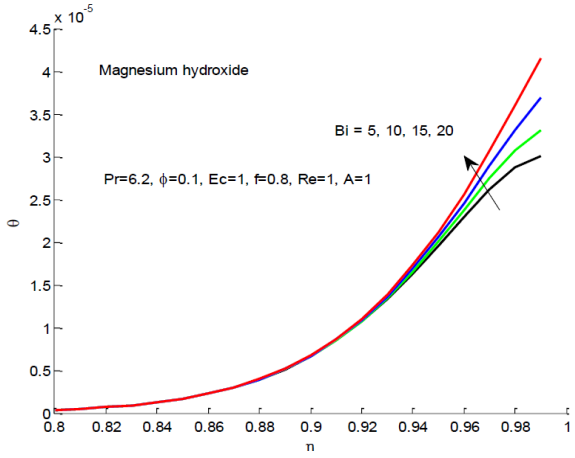

Fig. 9: Nanofluid temperature profiles with increasing Biot number (Bi)

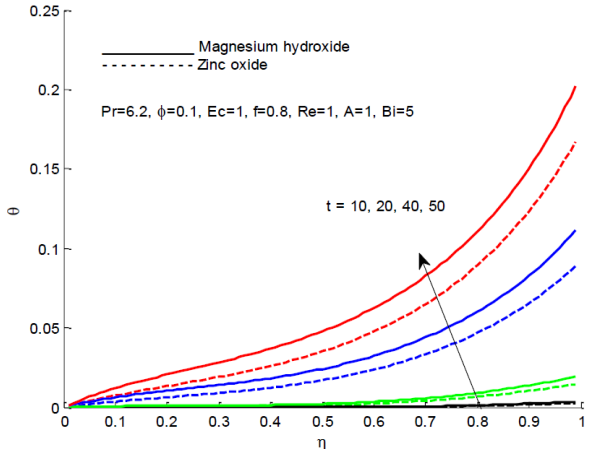

Fig. 8: Nanofluid temperature profiles across the channel with increasing time

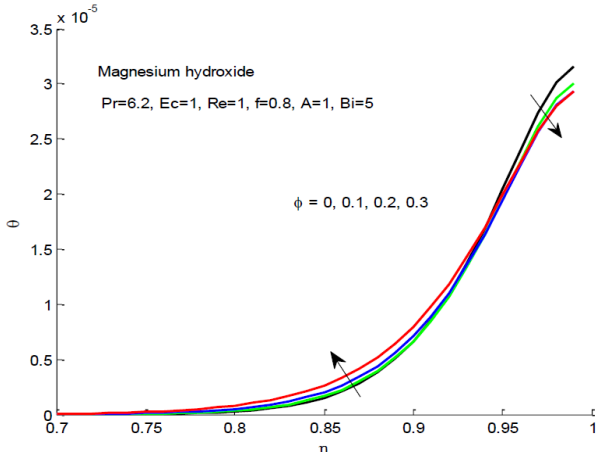

Fig. 10: Nanofluid temperature profiles with increasing ϕ

efficient energy utilization within the flow. In the context of fire suppression, this suggests that ZnO-based nanofluids can enhance heat removal efficiency, thereby improving cooling performance and contributing to more effective fire-extinguishing capability.

6 Skin Friction

Figure 13 shows the influence of pressure gradient (A) on skin friction within the upstream flow system. As the pressure gradient increases, the $Mg(OH)_2$-based nanofluid exhibits slightly lower skin friction compared to the ZnO-based nanofluid. This marginal difference can be attributed to variations in effective viscosity and flow resistance induced by the nanoparticle type. Although the reduction in skin friction for $Mg(OH)_2$ suggests a modest decrease in flow resistance and potentially lower pumping power requirements, the difference between the two nanofluids remains small. Therefore, while $Mg(OH)_2$ may offer a slight hydrodynamic advantage, its selection for fire extinguishing applications should be considered alongside other performance factors such as heat transfer efficiency, atomization characteristics, and overall thermodynamic behavior.

7 Conclusion

This study investigates fire-extinguishing efficiency using nanofluid flow through an upstream flow system. The nanofluid consists of magnesium hydroxide ($Mg(OH)_2$) and zinc oxide (ZnO) nanoparticles dispersed in water as the base fluid. The governing model equations are solved numerically in MATLAB using the

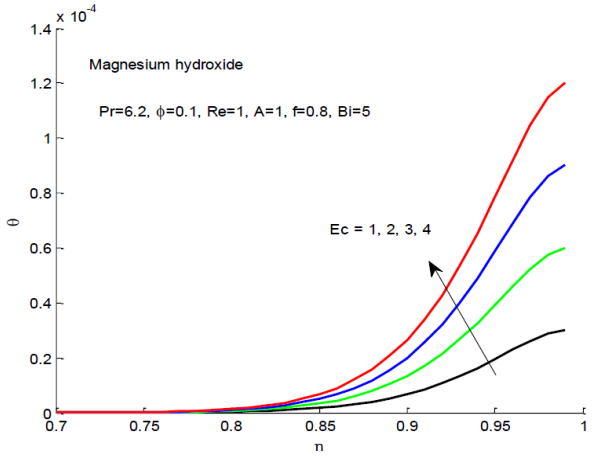

Fig. 11: Nanofluid temperature profiles with increasing Eckert Number (Ec)

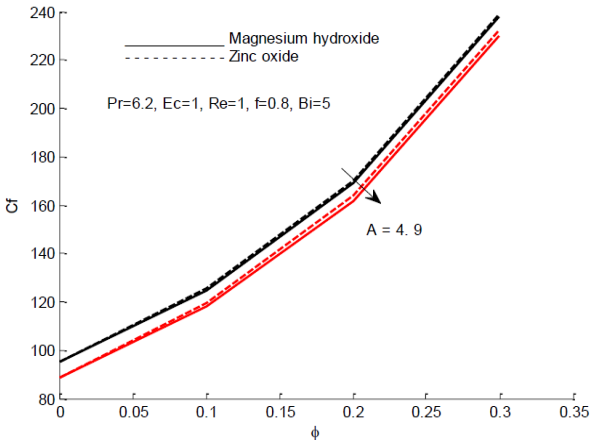

Fig. 13: Entropy generation with increasing ϕ

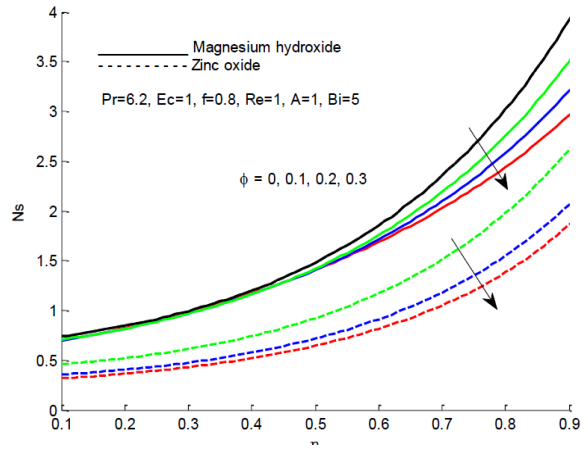

Fig. 12: Entropy generation with increasing ϕ

Runge–Kutta–Fehlberg scheme. The results reveal that velocity increases with time but decreases along the spatial coordinate for both magnesium hydroxide–water and zinc oxide–water nanofluids. Furthermore, the magnesium hydroxide–water nanofluid attains a higher velocity than the zinc oxide–water nanofluid. This behavior may be attributed to the comparatively lower thermal conductivity and higher specific heat of $Mg(OH)_2$, which reduces thermal diffusion and produces steeper temperature gradients, thereby indirectly influencing velocity through viscosity variations. The results also indicate that velocity decreases with increasing nanoparticle volume fraction due to the associated rise in fluid density and flow resistance.

However, the slip parameter in porous nanofluid systems is commonly treated as a constant boundary condition; however, this assumption may not fully capture the evolving nature of nanoparticle-laden flows. Nanoparticle deposition on the sprayer surface modifies the local roughness characteristics, thereby influencing near-wall momentum transfer. As the nanoparticle volume fraction increases, the likelihood of surface accumulation also increases, leading to enhanced roughness and a corresponding reduction in effective slip length.

It also shows that temperature increases with both time and space. Furthermore, the magnesium hydroxide-water nanofluid exhibits a higher temperature than the zinc oxide-water nanofluid, likely due to its distinct thermophysical properties. The temperature increases with both space and time. A marked difference in temperature elevation is observed between the two nanofluids, with the magnesium hydroxide-water mixture showing a more pronounced increase than the zinc oxide-water mixture a phenomenon likely due to its specific thermophysical properties. A higher Biot number (Bi) results in a nearly constant temperature profile, with a slight increase only near the upper plate. The increase in the nanoparticle volume fraction (ϕ) raises the temperature at the centerline but causes a slight decrease near the upper plate. Also indicates that a rise in the Eckert number (Ec) increases the temperature due to convective cooling at the upper wall.

Effects of different flow parameters, skin friction and entropy generation were investigated. The study identifies that magnesium hydroxide nanofluid acquire high velocity and temperature than zinc oxide. Furthermore, both nanofluids reduce entropy with an increase in nanoparticle fractions. Also, it is observed that there is a slight change in skin friction when using $Mg(OH)_2$ and ZnO nanofluid respectively. These findings play a critical role in determining the heat transfer performance of the nanofluid. In physically realistic systems, solid nanoparticles such as $Mg(OH)_2$ and ZnO possess higher thermal conductivity than the base fluid (water), leading to an increase in the effective thermal conductivity of the mixture. This enhancement facilitates more efficient heat

transport within the fluid and reduces temperature gradients. As a result, thermal entropy generation decreases, indicating reduced irreversibility and more effective utilization of thermal energy. In the context of fire suppression, this translates to improved heat extraction from the flame or heated surfaces, thereby accelerating cooling and enhancing extinguishing efficiency.

Acknowledgement

The authors are grateful to the anonymous referee for a careful checking of the details and for helpful comments that improved this paper.

References

[1] K. Farrell, M.K. Hassan, M.D. Hossain, B. Ahmed, P. Rahnamayiezekavat, G. Douglas, S. Saha., Fire **6** (2023).
[2] Z. Liu, A.K. Kim, Journal of Fire Protection Engineering **11** (2000).
[3] Q. Zhu, L. Wang, Y. Chen, H. Li, Fire Technology **56**, 2431–2452 (2020).
[4] M. Khudhair, A. Al-Janabi, R. Hassan, T. Salem, Journal of Hazardous Materials **441**, 129913 (2023).
[5] B. Kang, M. Marengo, S. Begg, Journal of Applied Fluid Mechanics **12** (2019).
[6] I. Razzaq, W. Xinhua, G. Rasool, T. Sun, A.S. Shflot, M.Y. Malik, et al., ACS Omega **10** (2025).
[7] H. Bellerová, A.A. Tseng, M. Pohanka, M. Raudensky, International Journal of Thermal Sciences **62** (2012).
[8] Y.T. Aksoy, H. Cornelissen, P. Eneren, M.R. Vetrano, Energies **16** (2023).
[9] Y.T. Aksoy, Y. Zhu, P. Eneren, E. Koos, M.R. Vetrano, Energies **14** (2021).
[10] J. Deng, Z. Hu, J. Chen, T. Deng, Y. Zhang, Z. Bai, et al., Journal of Energy Storage **106** (2025).
[11] N. Zhu, W.K. Chow, International Association for Fire Safety Science (2004).
[12] M. Sanches, G. Marseglia, A.P.C. Ribeiro, A.L.N. Moreira, A.S. Moita, Symmetry **13** (2021).
[13] A. Rabajczyk, M. Zielecka, J. Gniazdowska, Materials **15** (2022).
[14] Y.T. Aksoy, F. Enayati, P. Eneren, M.R. Vetrano, Applied Thermal Engineering **264** (2025).
[15] Y.T. Aksoy, Sustainability **17**, 8006 (2025).